A Universal Soft Switching Dual Active Bridge Converter for Electric Vehicle Charging Infrastructure towards Sustainable Electric Transportation

SARODE SHIVA KUMAR, AYYAGARI SAI LALITHA, GAURI SHANKER GUPTA
PANKAJ MISHRA, S. K. MISHRA
Department of Electrical and Electronics Engineering, Birla Institute of Technology Mesra, Ranchi, INDIA

Abstract: - This paper introduces a modified Dual Active Bridge (DAB) converter integrated with an LLC^2 resonant converter tailored for Electric Vehicle (EV) charging infrastructure, emphasizing a unidirectional power flow. The converter implements a two-stage power conversion process, leveraging the DAB's suitability for high-power applications characterized by enhanced efficiency, low voltage stress, and universal soft switching (ZVS) across all switches. Distinguishing itself from conventional isolated and non-isolated DC-DC converters, the DAB-LLC^2 configuration is systematically elucidated in terms of its operating principle, soft switching characteristics, steady-state attributes, output features and crucial design parameters. A meticulous design of a 3kW DAB-LLC^2 converter is conducted using MATLAB/Simulink software and the comprehensive results are documented, providing valuable insights into the converter's performance and applicability for EV charging infrastructure for sustainable electric transportation.

Key-Words: - DAB-LLC^2, soft switching, universal Zero Voltage Switching (ZVS), uni-directional power flow, Switching Frequency, Resonant Frequency

Received: February 15, 2024. Revised: August 27, 2024. Accepted: September 28, 2024. Published: October 16, 2024.

1. Introduction

The combustion of fossil fuels constitutes a significant contributor to the release of nitrogen oxide emissions, thereby amplifying adverse environmental impacts, including the formation of smog, acid rain, and the discharge of harmful gases. The adoption of renewable energy sources represents a comprehensive and viable solution to this challenge. By harnessing energy from renewable sources, the generation process is executed without emitting greenhouse gases, consequently mitigating air pollution. Furthermore, this transition to renewable energy not only addresses environmental concerns but also bolsters energy supply diversity, thereby reducing reliance on finite reserves of fossil fuels and promoting a more sustainable and resilient energy landscape.

Electric Vehicle Supply Equipment (EVSE), commonly referred to as an electric vehicle charging station, plays a pivotal role in establishing a crucial connection between electric vehicles, encompassing electric cars, neighborhood electric vehicles, and plug-in hybrids, and the electricity source for recharging. The charging infrastructure comprises three primary categories: Level 1, Level 2, and DC fast charging, each offering distinct power outputs. Notably, the utilization of DAB converters, renowned for their bi-directional current management capabilities, presents lightweight, efficient, and reliable solutions. However, higher operating frequencies result in increased losses, including conduction, gate, and body diode losses, thereby impacting overall efficiency and power output. In response to this, the adoption of the LLC^2 topology is employed to achieve ZVS in both primary and secondary switches, thereby enhancing system efficiency and augmenting power output.

In the papers, [4] - [6] introduces a semi dual active bridge converter featuring a symmetric bipolar output tailored for bipolar DC distribution systems. This innovative converter effectively addresses challenges related to pole voltage imbalance by incorporating a switched-capacitor circuit, thereby offering a combination of cost-efficiency and high-power conversion capabilities. A notable advantage of this design is the mitigation of the need for additional voltage balancing and feedback control in scenarios of unbalanced loads, resulting in reduced system complexity, fewer semiconductor

components, and diminished dependence on magnetic components.

Within the DAB configuration, multiple modulation techniques have been explored for the efficient management of soft switching [10] - [12]. These techniques include Single Phase Shift (SPS), Extended Phase Shift (EPS), Double Phase Shift (DPS), and Triple Phase Shift (TPS) respectively. Each of these modulation methods exhibits unique characteristics that significantly impact the operation and performance of the DAB configuration. Additionally, they interface with distinct control techniques [13] - [18]. The selection of a particular modulation strategy plays a pivotal role in determining the system's efficiency, control complexity, and overall performance within the DAB framework. Researchers and practitioners explore these modulation techniques to tailor the DAB operation to specific application requirements and optimize its functionality.

In this article, an enhanced open loop DAB converter has been introduced with LLC^2 topology, with the primary objective of mitigating switching losses and providing a symmetrical array of output voltage, specifically for the application of DC fast charging. A Pulse-Width Modulation (PWM) signal is systematically generated in which discrete pulses are delivered at uniform intervals, each pulse accompanied by a predetermined delay time.

Moreover, this enhancement in converter design is strategically directed towards optimizing and reducing the overall duration of the charging process. The subsequent sections of this article focus on a thorough and detailed investigation of these advancements. Through a comprehensive exploration of these developments, the article aims to elucidate their impact on charging efficiency, operational dynamics, and the broader implications for electric vehicle charging infrastructure. The meticulous examination of these innovations provides valuable insights into the evolving landscape of charging technologies, offering potential solutions to enhance the efficacy and feasibility of electric vehicle charging systems.

2. Problem Formulation

This section elucidates the configuration of the DAB-LLC^2 resonant converter. The operational sequence commences with the provision of a DC supply voltage, denoted as V_{in}, to a single-phase inverter. Subsequently, this inverter is intricately linked to a single-phase rectifier through the intermediary of a High-Frequency (HF) transformer. The primary function of the HF transformer lies in furnishing electrical isolation between the components of the converter, ensuring seamless and secure operation.

On the primary side of the transformer, integration with a resonant LLC circuit is established to realize soft switching attributes. The components comprising L_{pr} and L_p represent the resonant leakage and magnetizing inductances of the primary transformer, serving as the resonating inductors, while C_{pr} denotes the primary resonant capacitor interconnected in series. An additional LLC arrangement is implemented on the secondary side of the transformer. Here, L_s designates the secondary magnetizing inductance, aligned in series with a resonant inductor L_{sr}. Furthermore, a secondary resonating capacitor C_{sr} is interconnected in parallel, as illustrated in Fig. 1. Diodes D_1 and D_2 serve the purpose of delivering unidirectional current to the load.

The variables A_1 and A_2 denote angular disparities between S_{p1} and S_{s1}, and S_{p1} and S_{p3}, respectively, measured in radians. It is crucial to underscore that the operational switches can be systematically controlled to achieve a maximum phase difference of π radians. To streamline the analytical process, a duty cycle (D) of 0.5 has been implemented, facilitating a simplified and efficient approach to the system analysis.

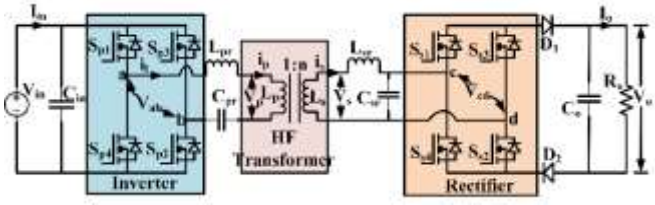

Fig. 1 Proposed DAB-LLC^2 resonant converter

In the context of this system, an inherent assumption is made regarding the ideal characteristics of all switches. Moreover, it is postulated that the capacitors utilized within the system exhibit adequate capacitance to sustain a consistent voltage level. Additionally, for the purpose of analytical simplification, the HF transformer is configured with a transformation ratio of 1:1. These assumptions collectively serve to streamline the theoretical framework, providing a foundational basis for the systematic analysis of the system's operational dynamics.

3. Problem Solution

3.1 Modes of operation

This section undertakes a comprehensive examination of the operating principle of the converter, portraying ten distinct modes of operation occurring within a single switching period. It is noteworthy that the first five modes bear resemblances to the subsequent five. Consequently, the discussion strategically centres on delivering an in-depth description of the first five modes, as they encapsulate the pivotal operational characteristics of the system. It is crucial to underscore the utilization of a specific sequencing strategy governing the operation of switches within the system. The initiation involves the simultaneous activation of switches S_{p1} and S_{p2}, followed by a deliberate delay before the engagement of switches S_{p3} and S_{p4}. This activation pattern is similarly implemented on the secondary side of the switches. With this carefully devised switching sequence, the subsequent explanation will demonstrate the modes of operation in this framework, providing a detailed examination of the distinct phases and its operations.

Mode 1 (t_o-t_1):

This interval serves as the dead time during which switches S_{p3} and S_{p4} undergo the transition from the ON to the OFF state, subsequently allowing for the activation of switches S_{p1} and S_{p2}. In this operational mode, the body diodes of switches S_{p1} and S_{p2} are intentionally turned ON, facilitating the establishment of a circulating current within the primary side current, denoted as i_p, carried over from the preceding cycle. This demonstrated sequence of events during the dead time period ensures the seamless transition between switch states and the controlled generation of the circulating current, thereby contributing to the system's operational continuity and efficiency.

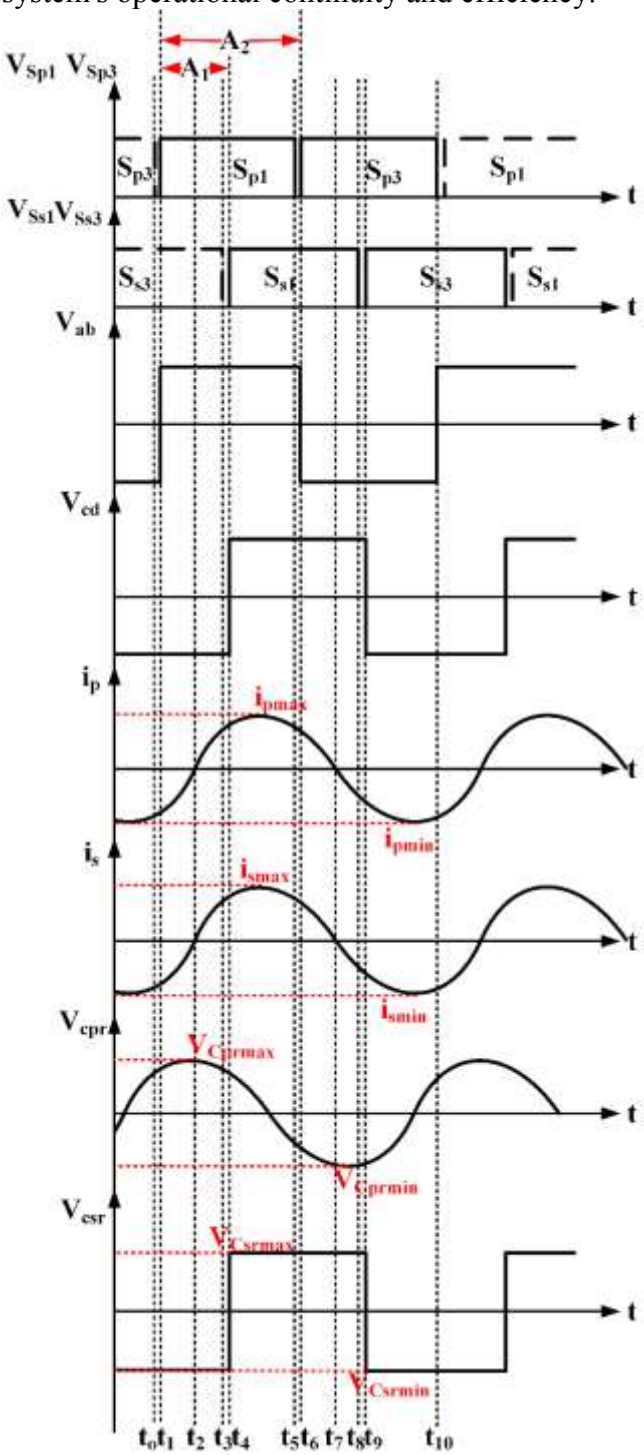

Fig. 2 Theoretical Waveforms of the proposed DAB-LLC resonant converter

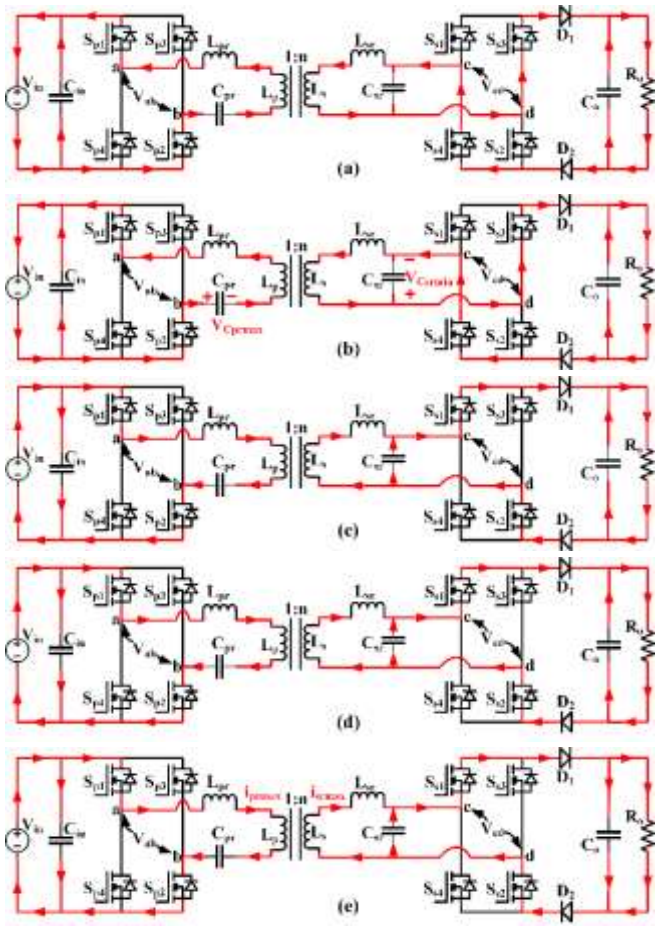

Fig. 3 Operational Modes of the proposed DAB-LLC Resonant Converter

$$i_p(t_1) = i_L(t_0) + \left(\frac{V_{in}}{Z} sin(w_o t_1)\right) * DT_s \quad (1)$$

$$V_{Cpr}(t_1) = V_{Cpr}(t_0) + \left(V_{in}(1 - cosw_o t_1)\right) * DT_s \quad (2)$$

$$V_{Co}(t_1) = V_{Co}(t_0) + \frac{V_o}{R_o C_o} DT_s \quad (3)$$

Mode 2: (t_1-t_2):

In this specific operational mode, the activation of primary switches S_{p1} and S_{p2} is turned ON, effectively achieving ZVS during the turn-on phase. Simultaneously, the current i_p, which flows in the reverse direction from the preceding cycle, undergoes demagnetization through the inductances L_{pr} and L_p until reaching a point of null amplitude. Concurrently, the capacitor C_{pr} undergoes charging, attaining a maximum voltage V_{Cprmax}. On the secondary side, switches S_{s3} and S_{s4} remain in the activated state, sustaining the flow of current, denoted as i_s, in the same direction as i_p, following the dot polarity convention. This operational configuration is represented in Figure 3(b). During this phase, the charging of the capacitor C_{sr} to C_{srmin} occurs. Consequently, the current supplied to the load undergoes a reduction and is supplemented by the energy stored in the capacitor C_o, contributing to the overall efficiency and dynamic performance of the system. The fundamental equations on the primary side are:

$$i_p(t_2) = i_L(t_1) + \left(\frac{V_{in}}{Z} sin(w_o t_2)\right) * DT_s \quad (4)$$

where,

$$Z = \sqrt{\frac{L_{eq}}{C_{pr}}}$$

$$w_o = \sqrt{\frac{1}{L_{eq} C_{pr}}}$$

$$L_{eq} = L_{pr} + L_p$$

$$V_{Cpr}(t_2) = V_{Cpr}(t_1) + \left(V_{in}(1 - cosw_o t_2)\right) * DT_s \quad (5)$$

$$V_{Co}(t_2) = V_{Co}(t_1) + \frac{V_o}{R_o C_o} DT_s \quad (6)$$

Mode 3 (t_2-t_3):

In this operational mode, the primary current i_p follows its conventional path, progressively increasing from zero, thereby magnetizing inductors L_{pr} and L_p. Simultaneously, the capacitor C_{pr} undergoes discharge through the circuit. On the secondary side, current flows through inductors L_{sr} and L_s, contributing to their magnetization. The capacitor C_{sr} retains its charged state with a maximum voltage. Towards the conclusion of this mode, switches S_{s3} and S_{s4} are consequently turned OFF, marking the culmination of this phase within the operational cycle. This orchestrated sequence of events within the mode contributes to the controlled magnetization of inductors, discharge of capacitors, and the strategic activation and deactivation of switches, collectively optimizing the energy flow and operational efficiency of the system.

$$V_{Co}(t_3) = V_{Co}(t_2) + \frac{V_o}{R_o C_o} DT_s \quad (7)$$

Mode 4 (t_3-t_4):

This operational mode allocates a specific dead time interval during which switches S_{s3} and S_{s4} undergo deactivation, creating an opportunity for the subsequent activation of switches S_{s1} and S_{s2}. In this phase, the intentional activation of the body diodes of switches S_{s1} and S_{s2}

occurs, facilitating the establishment of a circulating current within the secondary loop, as visually represented in Figure 3(d). This circulating current configuration is instrumental in sustaining the energy flow and ensuring a seamless transition between the activation and deactivation states of the switches, contributing to the overall operational continuity and efficiency of the system.

$$i_s(t_4) = i_s(t_3) + \left(\frac{V_{in}}{Z} sin(w_o t_4)\right) * DT_s \quad (8)$$

$$V_c(t_4) = V_c(t_3) + \left(V_{in}(1 - cosw_o t_4)\right) * DT_s \quad (9)$$

Mode 5 (t_4-t_5):

The operational sequence on the primary side of the DAB remains consistent with the preceding cycle. The capacitor C_{pr} undergoes discharge to reach a null voltage and subsequently begins charging in the opposite direction. Concurrently, on the secondary side, switches S_{s1} and S_{s2} are activated, implementing ZVS during the turn-on phase. The capacitor C_{sr} discharges from V_{Csrmin} to V_{Csrmax}, reaching its maximum voltage. During this phase, both primary and secondary currents, denoted as i_{prmax} and i_{srmax} respectively, attain their peak values. This orchestrated series of events contributes to the controlled energy transfer and dynamic performance of the DAB system, aligning with the specified operational objectives within the given cycle.

$$i_s(t_5) = i_s(t_4) + \left(\frac{V_{in}}{Z} sin(w_o t_5)\right) * DT_s \quad (10)$$

$$Z = \sqrt{\frac{L_{eq}}{C_{sr}}}$$

$$w_o = \sqrt{\frac{1}{L_{eq} C_{sr}}}$$

$$L_{eq} = L_{sr} + L_s$$

$$V_{csr}(t_5) = V_{csrmax}(t_4) + \left(V_{in}(1 - cosw_o t_5)\right) * DT_s \quad (11)$$

$$V_{Co}(t_5) = V_{Co}(t_4) + \frac{V_o}{R_o C_o} DT_s \quad (12)$$

3.1.1 Results and Discussion

3.1.1.1 Simulation Results

A 3kW DAB converter has been subjected to simulation using MATLAB/SIMULINK software platform, operating at a switching frequency of 100 kHz. In this simulation, four inductors are utilized, denoted by L_{pr}, L_{sr}, L_p and L_s of 15µH, 10µH and 720µH respectively with their capacitors C_{pr} and C_{sr} of 60nF and 5nF respectively.

The simulation results are effectively arranged through a series of graphical figures, with a particular emphasis on showcasing the soft switching characteristics of the converter. Four distinct diagrams are dedicated to illustrating this property, with a focus on two switches on the primary side and two on the secondary side. Specifically, Fig. 4 provides insights into the ZVS behavior of switch S_{p1}, while Fig. 5 captures the ZVS dynamics of switch S_{p3}. The subsequent representations in Fig. 6 and Fig. 7 depicts the ZVS property across the secondary switches, namely S_{s1} and S_{s3}. These results not only elucidate the ZVS phenomena in the highlighted switches but also extend to the remaining four switches, collectively showcasing the comprehensive ZVS behavior across the entire converter.

Fig. 8 provides a comprehensive representation of the primary and secondary current dynamics within the converter displaying high frequency sinusoidal behavior. Simultaneously, Fig. 9 captures the voltage behavior of both resonant capacitors, providing critical information on the energy storage and discharge patterns in the converter.

Fig. 10 depicts the terminal voltages of primary and secondary side of the converter, V_{ab} and V_{cd} respectively Fig. 11 portrays the output voltage and output current characteristics of the converter explaining the constant dc output voltage and current portraying the DC behavior in the output

Table 1. Parameter Selection of the Proposed Converter

Components	**Values**
Output power	3kW
Input voltage	200V
Switching Frequency	100kHz
Primary Resonant inductor, L_{pr}	15µH, 600V
Magnetized inductor	720µH,1000V
Primary Resonant capacitor, C_{pr}	60nF, 1000V
Secondary Resonant inductor, L_{sr}	10µH, 600V
Secondary Resonant capacitor, C_{sr}	5nF, 200V

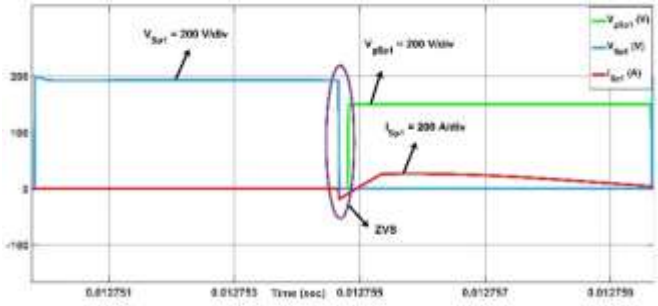

Fig. 7 Simulation result showing the ZVS behavior of switch S_{p1}.

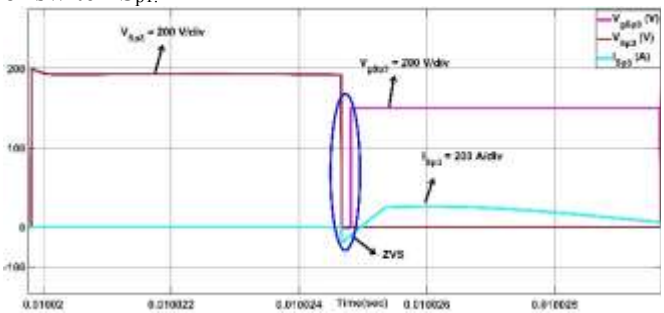

Fig. 8 Simulation result illustrating the ZVS behavior of switch S_{p3}.

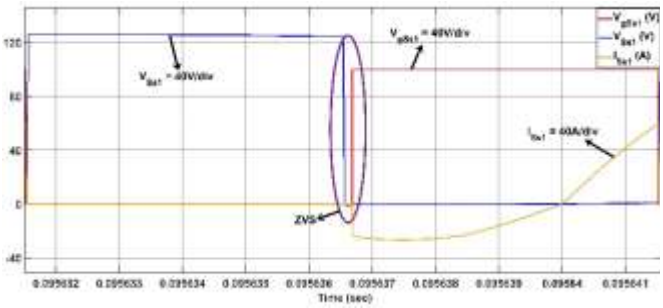

Fig. 9 Simulation result illustrating the ZVS behavior of switch S_{s1}

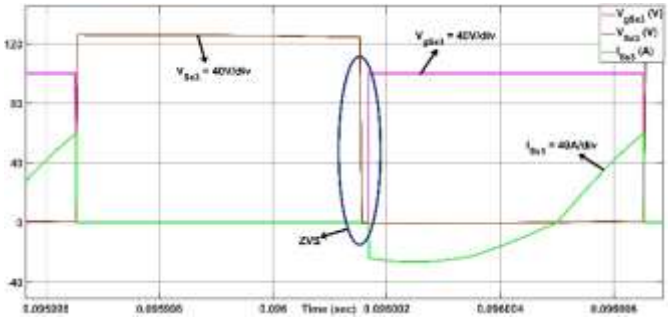

Fig. 10 Simulation result illustrating the ZVS behavior of switch S_{s3}

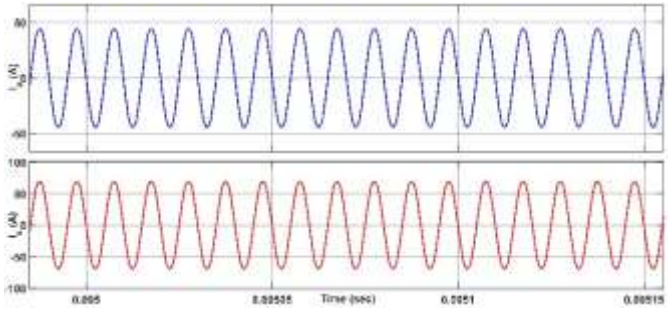

Fig. 11 Simulation result showing the primary current (i_p) and secondary current (i_s)

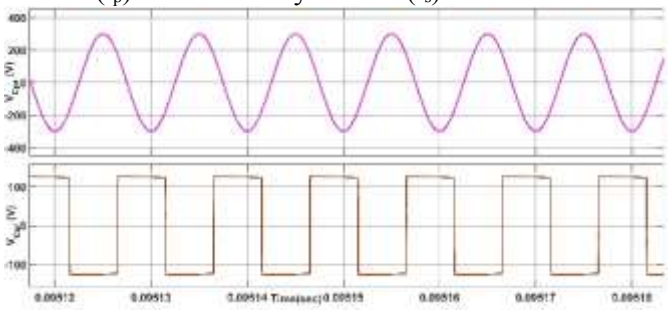

Fig. 12 Simulation result showing the primary resonant capacitor (C_{pr}) and secondary resonant capacitor (C_{sr})

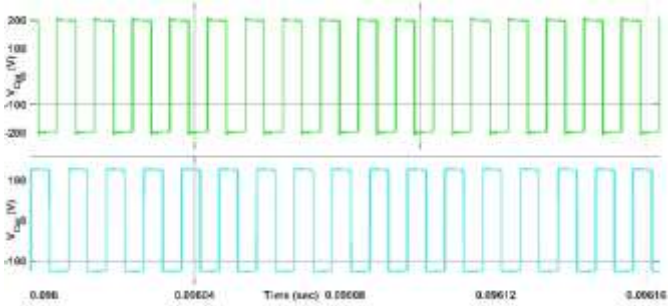

Fig. 13 Simulation result showing terminal voltages V_{ab} and V_{cd}

Fig 12 illustrates the efficiency curve of both the proposed DAB and a conventional DAB, offering a comparative analysis of their respective performance. The graphical representation evidently indicates a superiority in efficiency for the proposed DAB in comparison to the conventional counterpart.

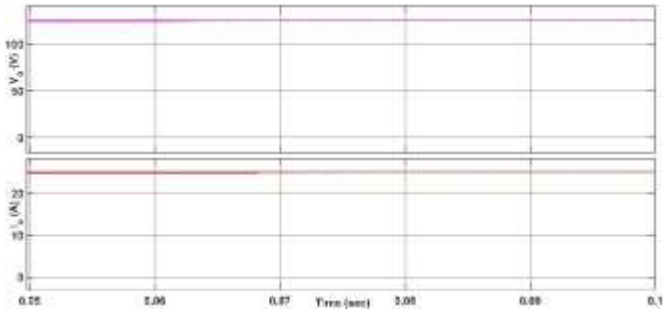

Fig. 14 Simulation result showing output voltage (V_o) and output current (I_o)

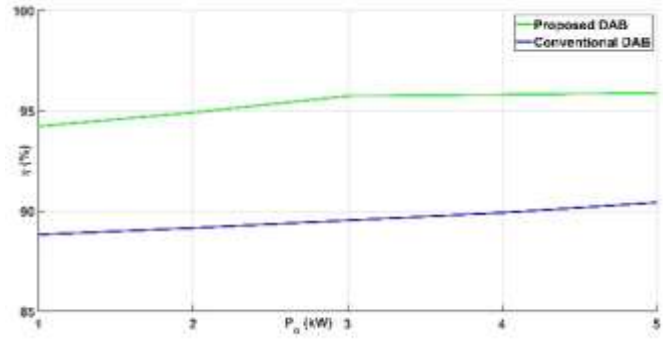

Fig. 15 Efficiency curve with respect to output power P_o

3.1.1.2 Hardware Results

A 3 kW DAB converter has been constructed for hardware implementation, operating at a switching frequency of 100 kHz.

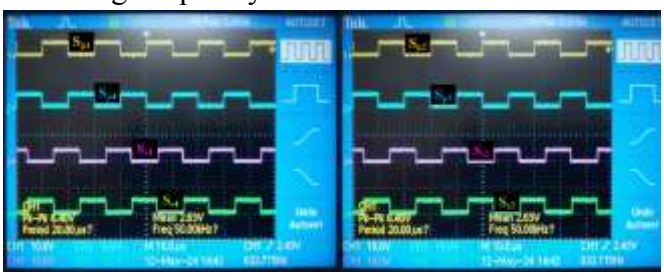

Fig. 17 Switching Pulses in all switches

Gate pulses for all switches are provided via the ATmega2560 microcontroller, as depicted in Fig. 17. The pulses are given at a switching frequency of 100 kHz with a dead time of 140 ns. The system parameters for the DAB-LLC[2] converter are detailed in Table 1.

The hardware figures obtained align with the expected outcomes and correspond well with the simulation results.

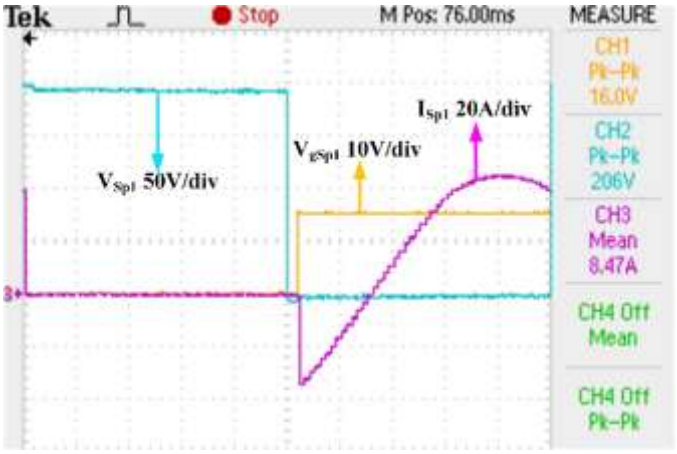

(a)

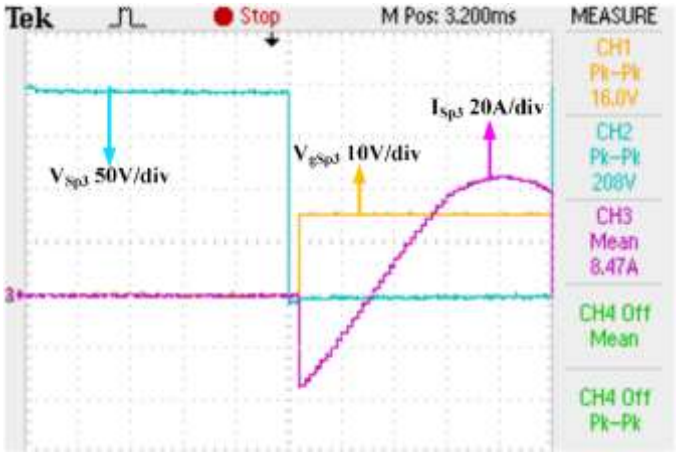

(b)

Fig. 18 Result depicting ZVS across (a) S_{p1} (b) S_{p3}

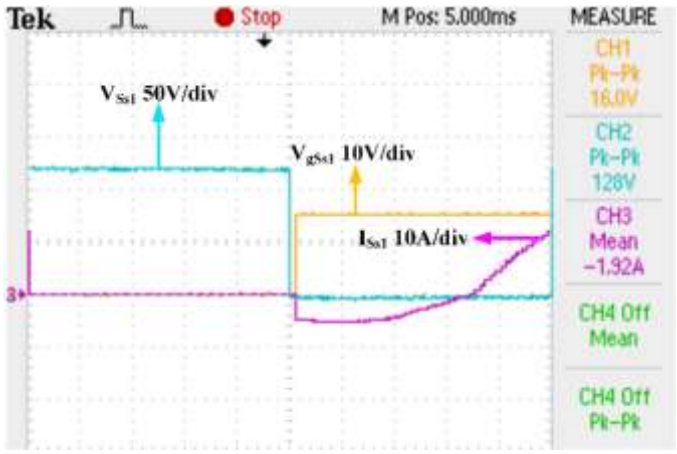

(a)

(b)

Fig. 19 Result depicting ZVS across (a) S_{s1} (b) S_{s3}

The figure illustrates the ZVS behavior across the primary switches. It demonstrates the soft switching behavior at switches S_{s1} and S_{s3}. The other switches exhibit similar characteristics to those shown in the figure. Hence proving universal soft switching across the entire converter.

Fig. 20 displays the primary and secondary currents across the transformer's primary and secondary windings, highlighting that the currents are in phase. Fig. 21 presents the voltage of the resonant capacitors on both the inverter and rectifier sides of the DAB-LLC^2 converter. Fig. 22 illustrates the transformer voltage across both the primary and secondary windings, describing the phase shift between the two signals that determines the phase shift ratio.

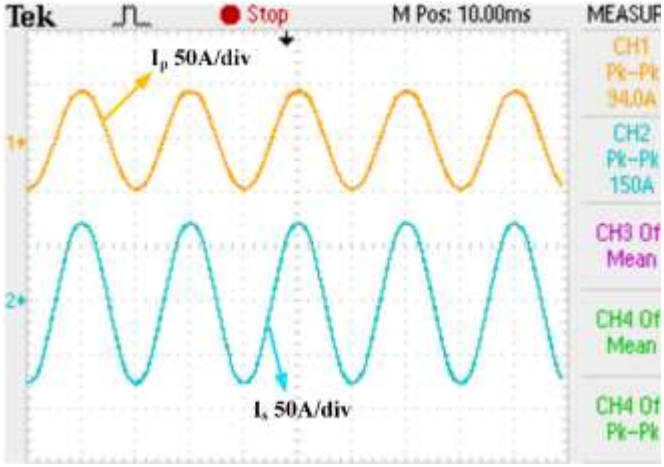

Fig. 20 Waveform of primary (i_p) and secondary (i_s) currents

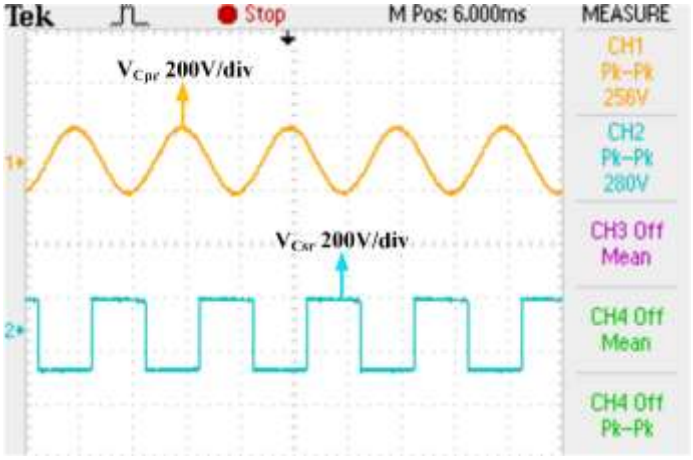

Fig. 21 Waveform depicting C_{pr} and C_{sr}

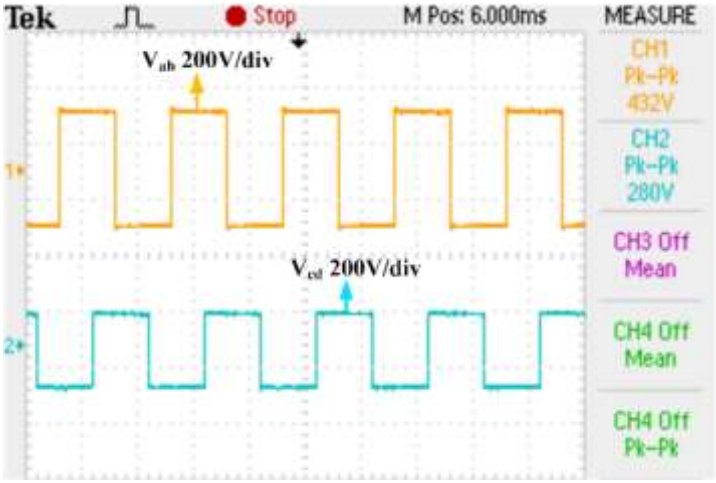

Fig. 21 Waveform transformer voltage V_{ab} and V_{cd}

Fig. 21 Waveform output voltage (V_o) and output current (I_o)

4. Conclusion

The paper introduces a novel DAB system that integrates seamlessly with an LLC^2 resonant converter, strategically designed to facilitate soft switching in both primary and secondary switches making it universal soft switching of

the proposed converter. Remarkably, the 3kW converter successfully fulfills a significant demand for current supply to the load, as depicted in the simulation and validated with experimental results. The integration of the LLC^2 resonant converter manifests a noticeable improvement in the overall quality factor, underscoring the efficacy of this innovative approach in optimizing performance and efficiency within the specified power range.

References:

[1] T. Yuvaraj, K. R. Devabalaji, S. B. Thanikanti, V. B. Pamshetti and N. I. Nwulu, "Integration of Electric Vehicle Charging Stations and DSTATCOM in Practical Indian Distribution Systems Using Bald Eagle Search Algorithm," *IEEE Access*, vol. 11, pp. 55149-55168, 2023.

[2] L. Li, G. Xu, D. Sha, Y. Liu, Y. Sun and M. Su, "Review of Dual-Active-Bridge Converters With Topological Modifications," *IEEE Transactions on Power Electronics*, vol. 38, no. 7, pp. 9046-9076, July 2023.

[3] J. -Y. Lee, H. -S. Kim and J. -H. Jung, "Enhanced Dual-Active-Bridge DC–DC Converter for Balancing Bipolar Voltage Level of DC Distribution System," *IEEE Transactions on Industrial Electronics*, vol. 67, no. 12, pp. 10399-10409, Dec. 2020.

[4] Q. Tian, X. Zhang, G. Zhou, H. Li and H. Ma, "Improved Dual Active Bridge DC–DC Converter With Symmetric Bipolar Output by Utilizing a Switched-Capacitor Circuit for Bipolar DC Distribution System," *IEEE Transactions on Industrial Electronics*, vol. 71, no. 1, pp. 524-536, Jan. 2024.

[5] J. -S. Hong, J. -I. Ha, S. Cui and J. Hu, "Topology and Control of an Enhanced Dual-Active Bridge Converter With Inherent Bipolar Operation Capability for LVDC Distribution Systems," *IEEE Transactions on Power Electronics*, vol. 38, no. 10, pp. 12774-12789, Oct. 2023.

[6] Z. Sun, Q. Wang, L. Xiao and Q. Wu, "A Simple Sensorless Current Sharing Control for Input-Parallel Output-Parallel Dual Active Bridge Converters," *IEEE Transactions on Industrial Electronics*, vol. 69, no. 11, pp. 10819-10833, Nov. 2022.

[7] C. Yu et al., "High Efficiency Bidirectional Dual Active Bridge (DAB) Converter Adopting Boost-Up Function for Increasing Output Power," *IEEE Transactions on Power Electronics*, vol. 37, no. 12, pp. 14678-14691, Dec. 2022.

[8] Z. Sun, Q. Wang, L. Xiao and Q. Wu, "A Simple Sensorless Current Sharing Control for Input-Parallel Output-Parallel Dual Active Bridge Converters," *IEEE Transactions on Industrial Electronics*, vol. 69, no. 11, pp. 10819-10833, Nov. 2022.

[9] O. Kircioğlu, M. Ünlü and S. Çamur, "The Comparison of Different Modulation Methods for Dual-Active-Bridge," *14th International Conference on Electronics, Computers and Artificial Intelligence (ECAI)*, Ploiesti, Romania, pp. 1-4, 2022.

[10] T. Liu, X. Ma, X. Hao, L. Huang, X. Yu and F. Duan, "A Comprehensive Modulation Scheme of DAB with Variable Voltage Gain," *4th International Conference on Energy, Electrical and Power Engineering (CEEPE)*, Chongqing, China, 2021.

[11] J. Tian, F. Wang, F. Zhuo and H. Deng, "Research on Multiple Duty Modulation Scheme in Dual-Active-Bridge-Based Energy Storage System," *IEEE Journal of Emerging and Selected Topics in Power Electronics*, vol. 11, no. 3, pp. 3562-3573, June 2023.

[12] J. Sun, L. Qiu, X. Liu, J. Zhang, J. Ma and Y. Fang, "Improved Model Predictive Control for Three-Phase Dual-Active-Bridge Converters With a Hybrid Modulation," *IEEE Transactions on Power Electronics*, vol. 37, no. 4, pp. 4050-4064, April 2022.

[13] N. Soltau, H. A. B. Siddique and R. W. De Doncker, "Comprehensive modeling and control strategies for a three-phase dual-active bridge," *International Conference on Renewable Energy Research and Applications (ICRERA)*, Nagasaki, Japan, 2012, pp. 1-6.

[14] F. Bagheri, N. Guler, H. Komurcugil and S. Bayhan, "An Adaptive Sliding Mode Control for a Dual Active Bridge Converter With Extended Phase Shift Modulation," *IEEE Access*, vol. 11, pp. 91260-91274, 2023.

[15] Y. Zhu et al., "Model Predictive Control With a Novel Parameter Identification Scheme for Dual-Active-Bridge Converters," *IEEE Journal of Emerging and Selected Topics in Power Electronics*, vol. 11, no. 5, pp. 4704-4713, Oct. 2023.

[16] A. Sai Lalitha, S. Chakraborty, S. S. Kumar, "An Efficient Soft Switching Synchronous Buck Converter for Battery Charging Application in Hybrid Electric Vehicle Architecture," *International Journal of Circuit Theory and Applications*, vol.51, no.11, pp.5154-5172, June. 2023.

[17] S. Li, X. Yuan, Z. Wang, K. Wang, Y. Zhang and X. Wu, "A Unified Optimal Modulation Strategy for DAB Converters to Tradeoff the Backflow Power Reduction and All ZVS in the Full Operating Range," *IEEE Journal of Emerging and Selected Topics in Power Electronics*, vol. 11, no. 6, pp. 5701-5723, Dec. 2023.

[18] Z. Lu, M. Su, G. Xu, L. Li, W. Xiong and J. Fang, "Switch-Multiplexed Quasi-Two-Stage Isolated Bidirectional Buck-DAB Converter with Full Load ZVS Range," *IEEE Transactions on Power Electronics*, vol. 38, no. 9, pp. 10541-10546, Sept. 2023.

Contribution of Individual Authors to the Creation of a Scientific Article

The authors equally contributed in the present research, at all stages from the formulation of the problem to the final findings and solution.

Sources of Funding for Research Presented in a Scientific Article or Scientific Article Itself

No funding was received for conducting this study.

Conflict of Interest

The authors have no conflicts of interest to declare that are relevant to the content of this article.

Creative Commons Attribution License 4.0 (Attribution 4.0 International, CC BY 4.0)

This article is published under the terms of the Creative Commons Attribution License 4.0
https://creativecommons.org/licenses/by/4.0/deed.en_US